iScience

CellPress

Article

Srv2 Is a Pro-fission Factor that Modulates Yeast Mitochondrial Morphology and Respiration by Regulating Actin Assembly

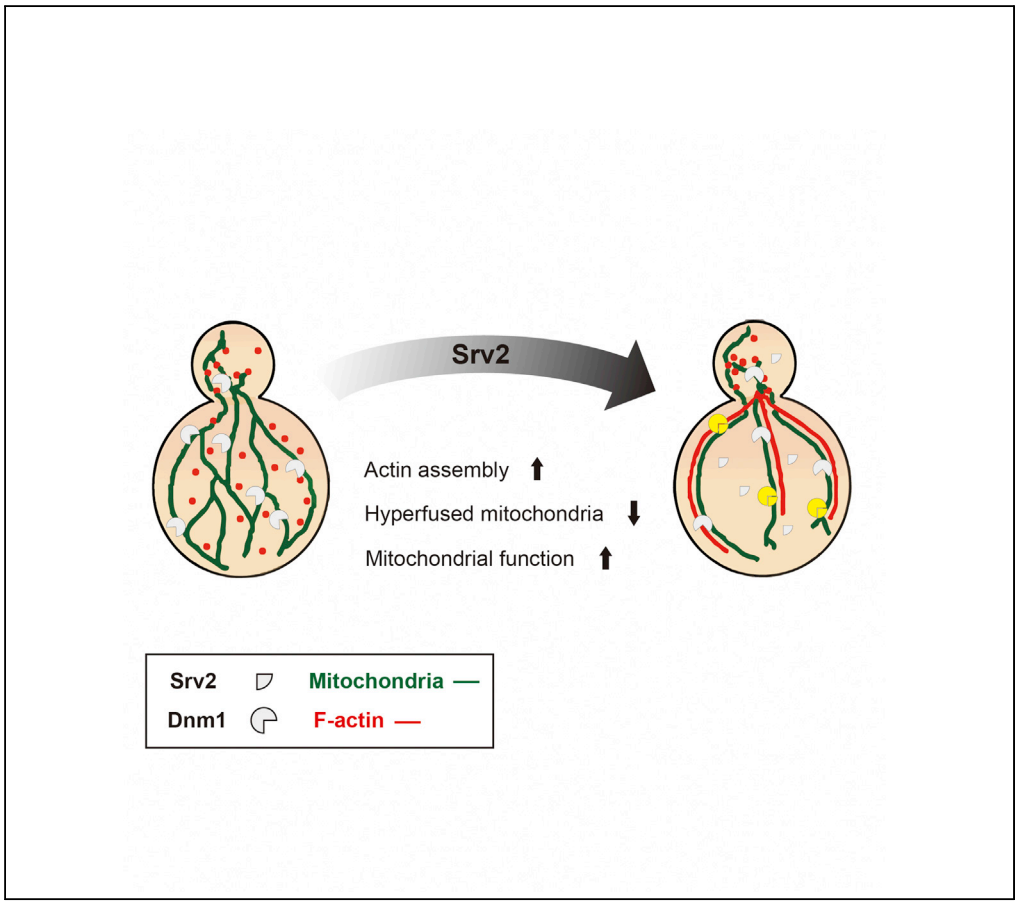

Ying-Chieh Chen, Tzu-Hao Cheng, Wei-Ling Lin, Chang-Lin Chen, Wei Yuan Yang, Craig Blackstone, Chuang-Rung Chang

blackstc@ninds.nih.gov (C.B.)
crchang@life.nthu.edu.tw (C.-R.C.)

HIGHLIGHTS

Srv2 interacts with fission protein Dnm1 on mitochondria in yeast cells

Srv2 deletion causes an irregular, hyperfused-elongated mitochondrial network

The irregular network derives from loss of Srv2-mediated actin assembly at mitochondria

Srv2 modulates both mitochondrial dynamics and activity

Chen et al., iScience *11*, 305–317
January 25, 2019
https://doi.org/10.1016/j.isci.2018.12.021

iScience

CellPress

Article

Srv2 Is a Pro-fission Factor that Modulates Yeast Mitochondrial Morphology and Respiration by Regulating Actin Assembly

Ying-Chieh Chen,[1] Tzu-Hao Cheng,[2] Wei-Ling Lin,[1] Chang-Lin Chen,[1] Wei Yuan Yang,[3] Craig Blackstone,[4,*] and Chuang-Rung Chang[1,5,*]

SUMMARY

Dynamic processes such as fusion, fission, and trafficking are important in the regulation of cellular organelles, with an abundant literature focused on mitochondria. Mitochondrial dynamics not only help shape its network within cells but also are involved in the modulation of respiration and integrity. Disruptions of mitochondrial dynamics are associated with neurodegenerative disorders. Although proteins that directly bind mitochondria to promote membrane fusion/fission have been studied intensively, machineries that regulate dynamic mitochondrial processes remain to be explored. We have identified an interaction between the mitochondrial fission GTPase Dnm1/DRP1 and the actin-regulatory protein Srv2/CAP at mitochondria. Deletion of Srv2 causes elongated-hyperfused mitochondria and reduces the reserved respiration capacity in yeast cells. Our results further demonstrate that the irregular network morphology in *Δsrv2* cells derives from disrupted actin assembly at mitochondria. We suggest that Srv2 functions as a pro-fission factor in shaping mitochondrial dynamics and regulating activity through its actin-regulatory effects.

INTRODUCTION

Mitochondria are critical organelles in eukaryotes. Among their known functions, the most significant is to produce energy for cells. Eukaryotic cells preferentially utilize mitochondria to produce ATP through oxidative phosphorylation, with oxygen as the final acceptor of electrons. In addition to its distinctive double membrane and undulating cristae structure, network dynamics also distinguish mitochondria from other organelles. The mitochondrial network is generated through continuous fusion, fission, trafficking, and anchoring. These complementary processes not only shape the network morphology but also aid in maintaining mitochondrial homeostasis and integrity. For instance, the fusion of mitochondria ameliorates functional defects and protects mitochondria from autophagic degradation during starvation (Gomes et al., 2011; Blackstone and Chang, 2011), and fission is critical for mitochondrial positioning and mitophagy (Youle and van der Bliek, 2012; Burman et al., 2017; Böckler et al., 2017).

Disruption of mitochondrial dynamics is correlated with mitochondrial disintegration. Neurons and muscle cells that require ATP for proper function are often prominently affected if mitochondrial function cannot be maintained. Models of Alzheimer, Parkinson, and Huntington diseases exhibit disrupted mitochondrial dynamics and irregular network morphology, prefiguring the importance of well-regulated mitochondrial dynamics (Cho et al., 2009; Shirendeb et al., 2012; Narendra et al., 2009).

Mitochondrial fusion and fission are evolutionarily conserved processes (Westermann, 2010), and large dynamin-related GTPases are required to drive both membrane fusion (MFN1/2 and OPA1) and fission (DRP1) in eukaryotes. In budding yeast, Fzo1 (yeast orthologue of mammalian mitofusins MFN1/2), Ugo1, and Mgm1 (yeast orthologue of OPA1) facilitate mitochondrial outer membrane fusion and inner membrane fusion cooperatively (Wong et al., 2000; Sesaki and Jensen, 2001; Hermann et al., 1998). Cytosolic Dnm1 (yeast orthologue of mammalian DRP1) is recruited to sites of mitochondrial fission by Fis1, Caf4, and Mdv1 to form a distinctive constriction ring (Griffin et al., 2005; Legesse-Miller et al., 2003; Chang and Blackstone, 2007). In addition to these proteins, the endoplasmic reticulum-mitochondria encounter structure (ERMES) is involved in the mitochondrial constriction process; the ER wraps around mitochondria at activated fission sites to facilitate mitochondrial division (Friedman et al., 2011). It appears

[1]Institute of Biotechnology, National Tsing Hua University, Life Science Building II, Room 506 No. 101, Section 2, Kuang-Fu Road, Hsin Chu City 30013, Taiwan, ROC

[2]Institute of Biochemistry and Molecular Biology, National Yang-Ming University, Taipei City 11221, Taiwan, ROC

[3]Institute of Biological Chemistry, Academia Sinica, Taipei City 11529, Taiwan, ROC

[4]Cell Biology Section, Neurogenetics Branch, National Institute of Neurological Disorders and Stroke, National Institutes of Health, Building 35, Room 2A-201, 9000 Rockville Pike, Bethesda, MD 20892, USA

[5]Lead Contact

*Correspondence: blackstc@ninds.nih.gov (C.B.), crchang@life.nthu.edu.tw (C.-R.C.)

https://doi.org/10.1016/j.isci.2018.12.021

that not all Dnm1 foci on mitochondria are activated fission sites, and more information is needed to clarify the differences between inactive and active Dnm1 foci.

Mitochondrial transport in *Saccharomyces cerevisiae* is highly dependent on actin filaments (Hermann et al., 1998; Huckaba et al., 2004; Fehrenbacher et al., 2004). A genetic screen for the essential genes involved in mitochondrial morphogenesis identified multiple actin cytoskeleton-associated proteins (Altmann and Westermann, 2005). In mammalian cells, actin filaments also play a role in ER-mitochondria contact-mediated fission; the dynamic assembly and disassembly of actin is critical for regulating mitochondrial fission (Hatch et al., 2014, 2016; Ji et al., 2015; Gurel et al., 2015; Li et al., 2015; Moore et al., 2016). However, detailed mechanisms of how actin is involved in mitochondrial dynamics remain unclear.

Evidence suggests that unidentified factors of mitochondrial dynamics still exist (Koch et al., 2004; Legesse-Miller et al., 2003). For instance, mitochondrial network morphology upon double deletion of the fusion protein Fzo1 and fission protein Dnm1 is similar to that of wild-type yeast, although double deletions still affect mitochondrial inheritance and cell survival rate (Böckler et al., 2017). In mammalian cells, mitochondrial constriction also requires multiple steps mediated by both DRP1 and classical dynamin-2 (Lee et al., 2016). These results indicate that more factors regulating mitochondrial fusion, fission, or both remain to be identified.

In this study, we report that Srv2/CAP interacts with the mitochondrial fission protein Dnm1/DRP1 and functions as a pro-fission factor. Srv2 was initially identified as a factor involved in cAMP/PKA signaling and actin assembly; it binds monomeric actin to sequester available G-actin (Freeman et al., 1995; Vojtek et al., 1991; Gerst et al., 1991). We found that Srv2 deletion causes the mitochondrial network to become hyperfused, likely reflecting its function in regulating actin filament assembly. In addition, the irregularly hyperfused mitochondrial network in *Δsrv2* cells is associated with lower reserve respiration capacity. Our finding that Srv2 functions as a pro-fission factor strengthens the argument for involvement of actin in mitochondrial fission and provides insight into the relationship between mitochondrial activity and network morphology.

RESULTS

Srv2/CAP Interacts with Dnm1/DRP1 at Mitochondria in Cells

To identify factors involved in mitochondrial dynamics, we performed yeast two-hybrid screening to search for potential factors that interact with the human mitochondrial fission protein DRP1 (splice variant 1, residues 1–736; Figure S1). Other than DRP1 itself, which is known to self-associate (Zhu et al., 2004), the only specific interactor identified was CAP2 (cyclase-associated protein 2). There are two CAP genes, CAP1 and CAP2, in mammalian cells. These two proteins have subtle differences in sequences along with different distributions (Peche et al., 2007). Based on phylogenetic analyses (Dereeper et al., 2010; Chevenet et al., 2006; Edgar, 2004; Guindon and Gascuel, 2003; Castresana, 2000), *S. cerevisiae* has only a single CAP orthologue, Srv2 (Figure 1A). Srv2 was originally identified as a protein required for RAS-activated adenylate cyclase activity and regulation of cAMP levels in yeast (Fedor-Chaiken et al., 1990). More recent studies have demonstrated that Srv2 binds actin and is required for normal actin turnover and organization (Chaudhry et al., 2010, 2014; Mattila et al., 2004; Balcer et al., 2003). Both cAMP signaling and the actin cytoskeleton have previously been identified to play important roles in mitochondrial dynamics (Li et al., 2015; Chang and Blackstone, 2007). Since a single CAP ortholog in yeast (Srv2) facilitates functional studies, we decided to investigate the role of CAP/Srv2 in mitochondrial dynamics and function in *S. cerevisiae* first.

We performed co-precipitation studies to confirm the interaction between Srv2 and Dnm1 in yeast. C-terminal Srv2 was conjugated with Tandem Affinity Purification tag (TAP-tag) in a Dnm1-HA yeast strain (Ghaemmaghami et al., 2003). Using calmodulin-affinity resin to precipitate Srv2-TAP, we demonstrated that Dnm1 co-precipitates with Srv2 (Figure 1B). The Srv2/Dnm1 co-precipitation was not seen in the Dnm1-HA only strain. In addition, we applied split-GFP-based bimolecular fluorescence complementation (BiFC) (Skarp et al., 2008) to examine the spatial and temporal interaction of Srv2 and Dnm1 *in vivo*. Dnm1-GFP 1–10 and Srv2-GFP 11 were expressed in yeast cells, and upon complementation we detected that more than 50% of cells contain reconstituted GFP puncta on mitochondria (Figure 1C). When we used either N- or C-terminal fragments instead of full-length Srv2 in BiFC experiments, C-terminal

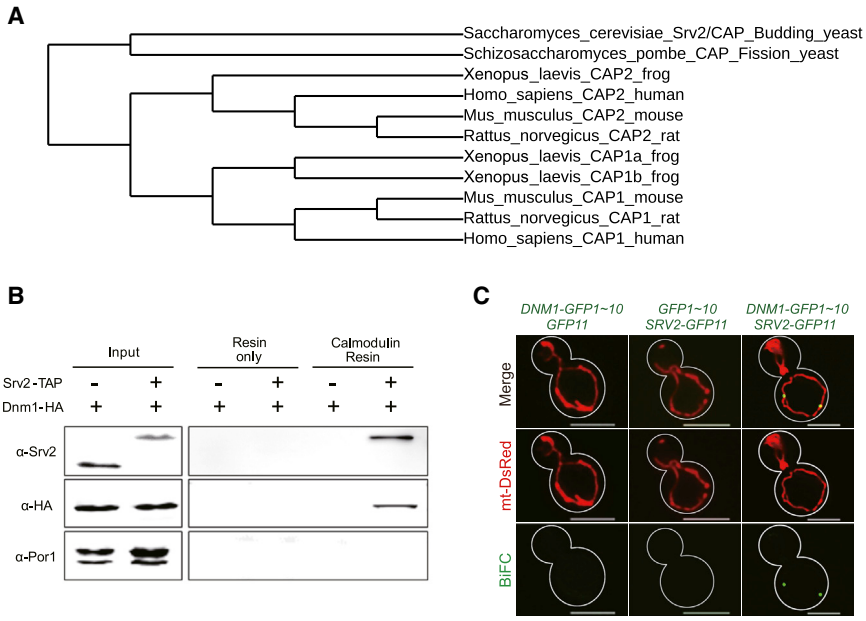

Figure 1. Yeast Srv2 Interacts with Mitochondrial Fission GTPase Dnm1

(A) Phylogenetic tree of Srv2/CAP proteins in different organisms.

(B) Srv2 was fused with the TAP tag, and Dnm1 was tagged with HA epitope. Following calmodulin-affinity chromatography, Srv2-Dnm1 co-precipitation was revealed by immunoblotting for HA. Porin was used as negative control. Note that the Srv2 antibody is less sensitive to Srv2-TAP than Srv2.

(C) Yeasts transformed with DNM1-GFP1∼10 + GFP11, GFP1∼10 + SRV2-GFP11, or DNM1-GFP1∼10 + SRV2-GFP11 were examined using the BiFC assay. mt-DsRed was expressed to label mitochondria. The BiFC signal of SRV2-GFP11 and DNM1-GFP1∼10 revealed the specific interaction of Srv2 with Dnm1 on mitochondria in living cells. Scale bars represent 5 μm.

Srv2 demonstrated complementary fluorescence puncta at mitochondria in cells (Figure S2). The co-precipitation and BiFC results indicate that Srv2 and Dnm1 interact with one other on mitochondria in living cells.

SRV2 Deletion Causes a Hyperfused Mitochondrial Network

To elucidate the functional role of Srv2 in mitochondrial dynamics, we used direct gene replacement to construct an *SRV2* deletion strain using the *KanMX* cassette (Figure 2A). Mitochondrial network morphology was used as an indicator for the status of mitochondrial dynamics. The mitochondrial network was labeled using mtGFP (Westermann and Neupert, 2000), and its morphology was classified into tubular, fragmented, and elongated-hyperfused categories by blinded observers. We found that 58% of *Δsrv2* cells exhibited an elongated-hyperfused mitochondrial network. In addition, these elongated-hyperfused mitochondria in *Δsrv2* cells had more branches as compared with the elongated mitochondria in fission-defect *Δdnm1* cells. By contrast, <10% of wild-type cells had elongated-hyperfused mitochondria (Figure 2B). To verify that the elongated-hyperfused mitochondrial phenotype was due to *SRV2* deletion, we examined mitochondrial morphology in an ectopic Srv2-expressing strain derived from the *Δsrv2* strain. Ectopically-expressed Srv2 efficiently complemented the phenotype of the *SRV2* deletion, and the ratio of cells with elongated-hyperfused mitochondria in cells ectopically expressing Srv2 approximated that of wild-type cells (Figures 2A and 2B). Next, we constructed a galactose-inducible Srv2 overexpression strain; the ratio of inducible *SRV2* cells with elongated-hyperfused mitochondria was close to that of *Δsrv2* cells in repressive dextrose medium. When yeasts were switched to galactose medium to induce Srv2 overexpression, the ratio of cells with elongated-hyperfused mitochondria was similar to that of the endogenously expressing cells (Figure 2C). Overexpression of Srv2 did not have any additional effects on mitochondrial structure or distribution. Together, these results demonstrate that the balance of mitochondrial fusion and fission in *Δsrv2* cells is shifted toward excess fusion, resulting in elongated-hyperfused mitochondria. Thus, data from *SRV2* deletion and galactose-induced overexpression of *SRV2* suggest that Srv2 is a pro-fission factor in yeast cells, particularly when combined with the data showing a direct interaction between Srv2 and Dnm1.

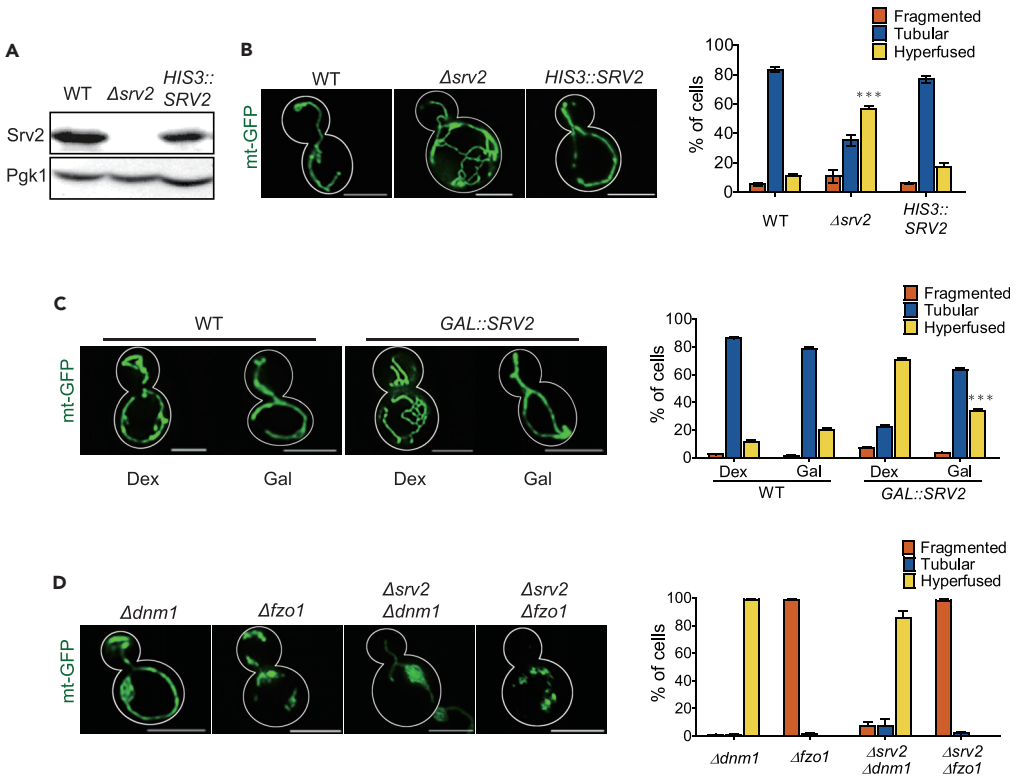

Figure 2. Srv2 Is Required for Maintaining Mitochondrial Dynamics

(A) *SRV2* deletion and ectopic expression (*HIS3::SRV2*) were confirmed by immunoblotting, with Pgk1 as a protein loading control.

(B) Mitochondrial network morphology in wild-type, *Δsrv2*, and *HIS3::SRV2* cells expressing mtGFP was examined by fluorescence microscopy. In the right panel, the mean ratios of cells with hyperfused mitochondria were: wild-type, 11.33%; *Δsrv2*, 56.67%; and *HIS3::SRV2*, 17.33%. Statistical data for each strain or condition were obtained from three trials of 100 yeast cells. The mean values ±SE were obtained by averaging the percentages of three counts. ***$p < 0.001$ vs. wild-type group. Scale bars represent 5 μm.

(C) Effects of ectopic Srv2 induction on mitochondria were examined with *GAL::SRV2* cells. The ratio of cells with hyperfused mitochondria in YPDex vs. YPGal medium was: wild-type, 11.67% vs. 20%; *GAL::SRV2*, 70.67% vs. 33.67%. ***$p < 0.001$ vs. Dex group.

(D) Mitochondria network classification for *Δdnm1*, *Δfzo1*, *Δsrv2 Δdnm1*, and *Δsrv2 Δfzo1* strains. *SRV2* depletion had no synergic effects on the mitochondrial morphology in the *FZO1* or *DNM1* deletion strains.

To clarify further the role of well-known mitochondrial fusion/fission factors in generating the hyperfused mitochondrial phenotype in *Δsrv2* cells, we examined mitochondrial network morphology in several double-deletion yeast strains, *Δsrv2 Δdnm1* and *Δsrv2 Δfzo1*. Removal of the *SRV2* gene in combination with the mitochondrial fission factor *DNM1* or fusion factor *FZO1* did not reveal synergic effects (Figure 2D); mitochondrial network morphology in double-deletion strains remained elongated-hyperfused in *Δsrv2 Δdnm1* cells and fragmented in *Δsrv2 Δfzo1* cells. Collectively, the mitochondrial morphologies in single- and double-deletion strains indicate that these conventional fusion/fission GTPases are decisive factors in generating mitochondrial morphology in *Δsrv2* cells.

Dnm1 Localization Is Not Affected by SRV2 Deletion

Dnm1 is a cytosolic protein recruited to fission sites on mitochondria to form a fission complex, constricting mitochondria and driving their fission (Kuravi et al., 2006; Griffin et al., 2005; Mozdy et al., 2000). The BiFC assay already demonstrated that Srv2 and Dnm1 interact with one another on mitochondria. To explore the possibility that deletion of *SRV2* affects translocation of Dnm1 to mitochondria and reduces fission complex formation, we examined protein levels of Dnm1 in the mitochondrial fraction. Dnm1 protein levels in mitochondrial fractions isolated from both wild-type and *Δsrv2* cells were similar, although a slightly lower

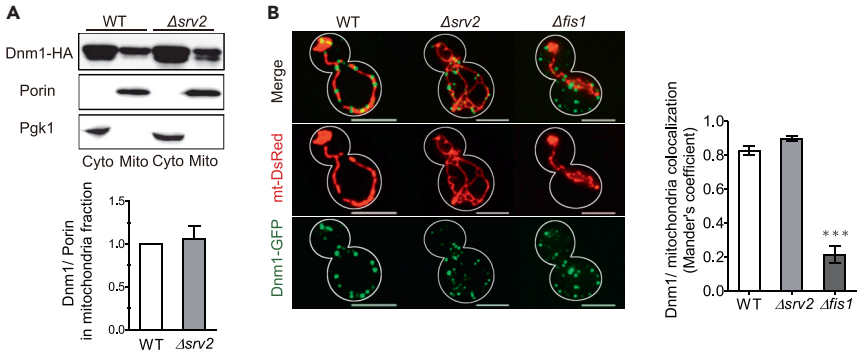

Figure 3. *SRV2* Deletion Does Not Affect Dnm1 Distribution

(A) Dnm1-HA levels in mitochondrial and cytosolic fractions of wild-type (WT) and *Δsrv2* cells were evaluated by immunoblotting. Pgk1 and porin were used as cytosolic (Cyto) and mitochondrial (Mito) markers, respectively. Mitochondrial Dnm1 levels were normalized to porin levels for comparisons. Mean ± SD from three trials are presented. (B) Wild-type, *Δsrv2*, and *Δfis1* cells expressing mt-DsRed and Dnm1-GFP were imaged by fluorescence microscopy. Dnm1-GFP foci on mt-DsRed were analyzed using ImageJ software. Mander's coefficient indicates the degree of association of Dnm1-GFP and mt-DsRed. ***$p < 0.001$ vs. WT group. Means ±SD are presented; 25 yeast cells/strain. Scale bars represent 5 μm.

molecular weight form of Dnm1 was more notable in the *Δsrv2* cells (Figure 3A). We labeled mitochondria and Dnm1 with different fluorescence proteins, and the localization of Dnm1 foci at mitochondria was assayed using Mander's colocalization coefficient method (Li et al., 2015; Dunn et al., 2011). We found that *SRV2* deletion did not affect the colocalization of Dnm1 and mitochondria. On the other hand, *FIS1* deletion dramatically decreased the localization of DNM1 puncta to mitochondria (Figure 3B). Thus, it is unlikely that Srv2 depletion affects Dnm1 recruitment to mitochondria.

Srv2 Function in Actin Dynamics Is Required for Shaping Mitochondria

Since Dnm1 levels and foci numbers at mitochondria are not affected by *SRV2* deletion, it seemed more likely that the elongated-hyperfused mitochondrial phenotype in *Δsrv2* cells emanated from loss of a specific Srv2 function. The N-terminal domain of Srv2 has been reported to be involved in cAMP/PKA signaling, and the C-terminal domain is involved in regulating actin dynamics. Overexpression of N-terminal and C-terminal Srv2 fragments can complement cAMP/PKA signaling and rescue defects in actin dynamics in *Δsrv2* cells, respectively (Chaudhry et al., 2010, 2014; Mattila et al., 2004; Balcer et al., 2003; Fedor-Chaiken et al., 1990). Overexpression of N- or C-terminal Srv2 fragments in *Δsrv2* cells was then used to examine which half of Srv2 could reverse the elongated-hyperfused phenotype and restore mitochondria to a more typical tubular morphology (Figure 4A). Overexpression of C-terminal Srv2 caused 36.67% cells to have elongated-hyperfused mitochondria. However, 57.67% of cells with empty vector and 60.33% of cells with overexpressed N-terminal Srv2 contained elongated-hyperfused mitochondria with the *Δsrv2* background. The results demonstrated that overexpression of C-terminal Srv2 has the ability to rescue the mitochondrial phenotype in *Δsrv2* cells (Figure 4B). These data also suggest that the function of Srv2 in actin assembly is important for mitochondrial dynamic processes.

To examine further the role of actin assembly in mitochondrial network shape, we overexpressed yeast profilin (Pfy1), an actin monomer-binding protein that is critical for actin organization, in *Δsrv2* cells (Yoshida et al., 2013; Sagot et al., 2002; Haarer et al., 1990). Pfy1 overexpression compensates for defects of actin dynamics (Magdolen et al., 1993; Vojtek et al., 1991). When Pfy1 was expressed in *Δsrv2* cells, 36.33% of cells contained elongated-hyperfused mitochondria. This number was reduced to a level similar to those cells overexpressing the C-terminal fragment of Srv2 (Figure 4B). Based on the complementation results of yeasts overexpressing the C-terminal domain of Srv2 and full-length Pfy1, Srv2-mediated mitochondrial dynamics appears closely associated with its role in regulating actin dynamics.

Disrupted Srv2-Mediated Actin Dynamics Cause Morphological Changes in the Mitochondrial Network

Two *SRV2* mutant alleles, *srv2-91* and *srv2-98,* cause actin severing and actin recycling defects, respectively (Chaudhry et al., 2010, 2013). To clarify how Srv2 affects mitochondrial dynamics through its

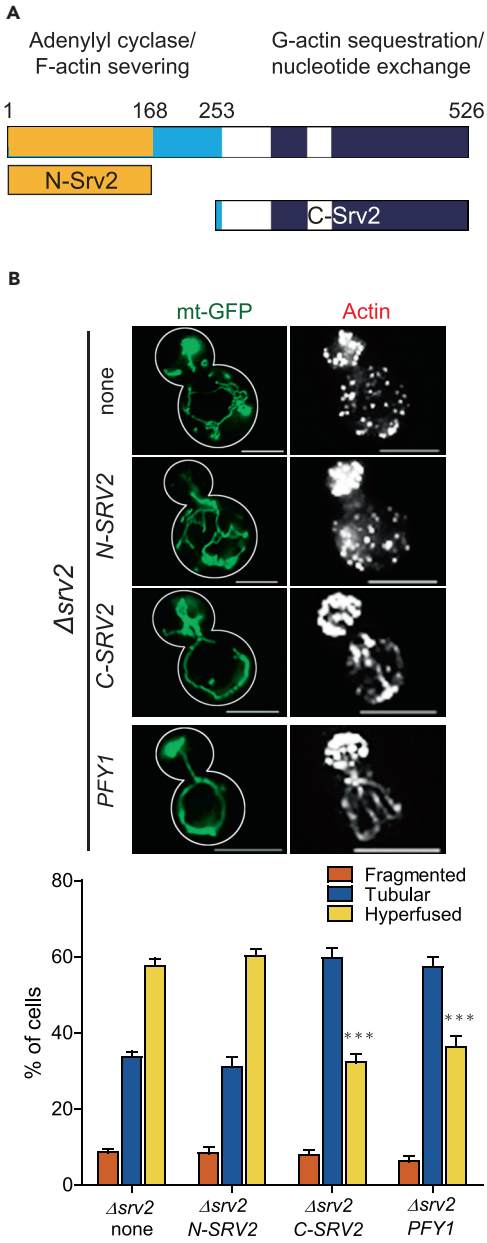

Figure 4. Complementary Experiments Indicated Srv2's Function in Actin Is Critical for Regulating Mitochondria Dynamics

(A) Schematic diagram of Srv2 showing key domains and truncations used in these experiments. Amino acid residue numbers are across the top.

(B) Morphology of mitochondria and F-actin in *Δsrv2* cells overexpressing the indicated Srv2 truncations were visualized by fluorescence microscopy. Ratios of cells with hyperfused mitochondria in *Δsrv2* yeast transformed with empty vector (none), N-SRV2, C-SRV2, and PFY1 were 57.67%, 60.33%, 36.67%, and 36.33%, respectively. ***$p < 0.001$ vs. empty vector (none) group. Mitochondrial morphology data in each strain were collected from three trials of 100 yeast cells, with means ±SE plotted. Scale bars represent 5 μm.

role in regulating actin dynamics, we examined mitochondrial network morphology in yeast strains harboring the *srv2-91* and *srv2-98* mutant alleles (Figure 5A). The ratio of cells with an elongated-hyperfused mitochondrial network in both strains (37.00% and 26.67%, respectively) was significantly higher than the 11.33% in wild-type yeast cells (Figure 5B). Another mutant allele, *srv2-189* (Figure 5A), harbors mutant properties of both *srv2-91* and *srv2-98*, and 63.00% of *srv2-189* cells contained

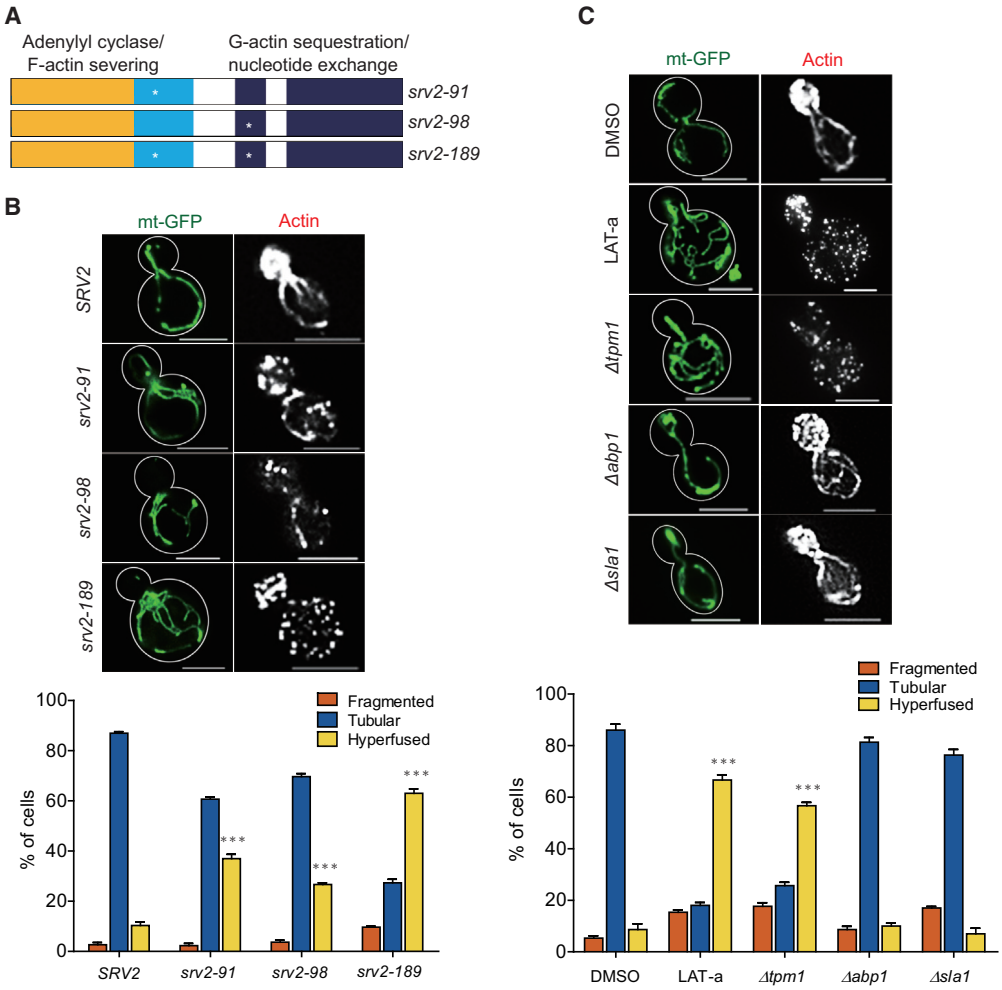

Figure 5. Srv2 Regulates Fission by Modulating Actin on Mitochondria

(A) Schematic diagram showing the *SRV2* mutant yeast alleles used in these experiments.

(B) Effects of *srv2* mutant alleles on mitochondrial network morphology and F-actin assembly were examined using fluorescence microscopy. Ratios of cells with hyperfused mitochondria in *SRV2*, *srv2-91*, *srv2-98*, and *srv2-198* strains were 10.33%, 37%, 26.67%, and 63.00%, respectively. ***$p < 0.001$ vs. *SRV2* cells.

(C) Analyses of mitochondrial morphology and F-actin in wild-type (WT) cells treated with latrunculin A along with mutant stains of *Δtpm1*, Δ*abp1*, and Δ*sla1* cells were used to verify the effects of F-actin assembly on mitochondrial dynamics. Mitochondrial morphologies for each strain or condition were analyzed from three independent counts of 100 yeast cells. ***$p < 0.001$ vs. dimethylsulfoxide-treated cells or WT cells. Mean values ±SE were obtained by averaging the percentages of three independent counts. Scale bars represent 5 μm.

elongated-hyperfused mitochondria. This ratio in *srv2-189* was very similar to that of the *Δsrv2* strain (Figure 5B).

Our results thus far suggest that actin-related functions of Srv2 are critical for its modulation of mitochondrial dynamics. To clarify the role of actin in regulating mitochondrial fusion and fission, we treated wild-type yeast with latrunculin A, a compound that sequesters G-actin and inhibits actin polymerization. We found mitochondria network morphology has dose-dependent alteration in response to latrunculin A. Low dosage of latrunculin A treatment caused hyperfused mitochondrial network, whereas high dosage caused fragmented mitochondria. Treatment of cells with 0.5 μM latrunculin A caused three phenotypes—isotropic growth, fewer actin cables, and hyperfused mitochondria—all of which are reminiscent of *Δsrv2* phenotypes (Figure 5C). To our surprise, both co-precipitation and BiFC results demonstrated that the Srv2/Dnm1 interaction was not affected, whereas actin polymerization was inhibited under the

same latrunculin A treatment condition (Figure S3). Thus, our data demonstrate that actin filament/cable assembly at mitochondria is important for maintaining mitochondrial dynamics in yeast cells.

We next constructed a tropomyosin (*TPM1*) deletion strain; Tpm1 is a protein that binds to and stabilizes actin cables and filaments (Liu and Bretscher, 1989). In the *Δtpm1* strain, we found that 56.67% cells exhibited an elongated-hyperfused mitochondrial network (Figure 5C). However, deletion of two cortical actin-binding proteins, *ABP1* (*A*ctin *B*inding *P*rotein) and *SLA1* (*S*ynthetic *L*ethal with *A*BP1), did not cause elongated-hyperfused mitochondria (Figure 5C). Both Abp1 and Sla1 are important for actin patch formation. We examined actin cable in these mutant strains by phalloidin staining (Figure 5) and quantified actin cable numbers based on previous studies (Alioto et al., 2016; Higuchi-Sanabria et al., 2016). The *Δtpm1* strain has almost no visible actin cables, whereas *Δsrv2* and *srv2-189* strains have similar actin cable counts that are lower than those of *srv2-91* and *srv2-98* strains. Both Δ*abp1* and Δ*sla1* strains demonstrated minor reduction of actin cable counts compared with wild-type cells (Figure S4). These results from genetic deletion strains, along with data from latrunculin A-treated cells and the *Δsrv2* cells, demonstrate that Srv2-mediated actin filament/cable assembly rather than patch formation is more important for maintaining the balance of mitochondrial dynamics.

We also examined the effects of CAP2 deletion on mitochondria in SH-SY5Y cells. Applying CRISPR/Cas9 to delete both alleles of CAP2, we found that a majority of CAP2$^{-/-}$ cells bear a hyperfused mitochondrial network (Figure S5). The CAP2 knockout cells demonstrated that Srv2/CAP2 is important for mitochondrial fission in both mammalian and yeast cells.

Deletion of SRV2 Affects Mitochondrial Activity

Changes in mitochondrial dynamics are closely associated with adjustments in mitochondrial activity. For instance, Parkin/Pink1 respond to a reduced mitochondrial membrane potential to promote mitochondrial fission (Jin and Youle, 2012; Narendra et al., 2010), and elongation of mitochondria helps to preserve their membrane potential during nutrient starvation (Blackstone and Chang, 2011; Gomes et al., 2011). As *SRV2* deletion causes elongation and hyperfusion of the mitochondrial network, it is plausible that mitochondrial activity would not be the same as that of wild-type cells. A high-resolution respirometer (Oroboros Oxygraph 2K) was used to examine the oxygen consumption rate, elucidating the mitochondrial reserve respiration capacity. We treated cells with compounds that inhibit oxidative phosphorylation at different stages of electron transport: triethyltin bromide (TET) to inhibit ATP synthase, carbonyl cyanide-4-(trifluoromethoxy)phenylhydrazone (FCCP) to increase proton permeability across the mitochondrial inner membrane, and antimycin to inhibit complex III. Oxygen consumption under the stress induced by these pharmacological agents was recorded throughout the procedure. Oxygen consumption rates during each step of the chemical treatments were normalized to flux control factor values to elucidate the reserve respiration capacity (Figure S6). Our results demonstrate that *Δsrv2* and *srv2-189* cells have a lower reserve respiration capacity as compared with wild-type and *Δdnm1* cells (Figure 6A).

Owing to catabolite repression in the presence of dextrose, mitochondrial activity would be de-repressed when yeast cells switch to a non-dextrose medium (Gancedo, 1998). To verify further the reserve respiration capacity results, we examined the routine oxygen consumption rate of wild-type, *Δdnm1*, *Δsrv2*, and *srv2-189* cells in both dextrose and non-dextrose (raffinose) medium (Figure 6B). All four strains had higher oxygen consumption rates in raffinose than dextrose. We then examined the mitochondrial membrane potential in both dextrose and raffinose media, applying $DiOC_6$ to detect the mitochondrial membrane potential using flow cytometry. Cells cultured in raffinose had a higher membrane potential than those cultured in dextrose (Figure 6C). An intriguing finding was that raffinose-related increases in the levels of oxygen consumption and membrane potential in both *Δsrv2* and *srv2-189* strains were lower than in wild-type and *Δdnm1* cells (Figures 6B and 6C). These membrane potential and oxygen consumption rate results are consistent with the reserve respiration capacity results. Together, these data demonstrate that Srv2 defects not only change the mitochondrial network morphology but also impact mitochondrial activity, especially the reserve respiration capacity.

DISCUSSION

SRV2 deletion and mutant alleles cause elongated-hyperfused mitochondria, and this phenotype can be reverted by the overexpression not only of Srv2 but also of Pfy1, indicating that Srv2 modulates

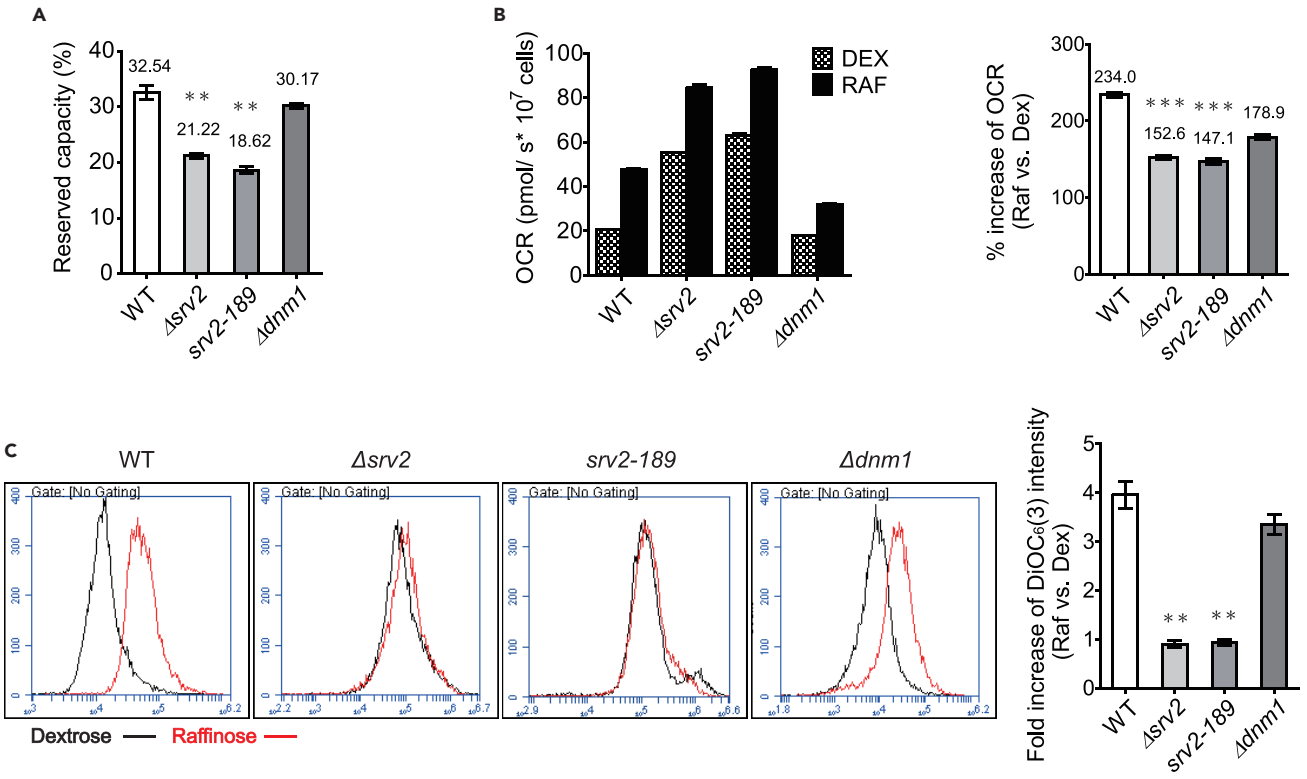

Figure 6. Mitochondrial Activity Is Altered by *SRV2* Deletion

(A) High-resolution respirometry was used to assay the oxygen consumption rate (OCR) as described in Methods. OCRs of wild-type, *Δsrv2*, *srv2-189*, and *Δdnm1* yeast in YPD with mitochondrial respiration complex inhibitors were determined (Figure S6). Reserve capacities (1-Routine respiration/maximal respiration) of wild-type, *Δsrv2*, *srv2-189*, and *Δdnm1* mitochondria were 32.54%, 21.22%, 18.62%, and 30.17%, respectively. **p < 0.01 vs. WT cells. (B) OCRs for wild-type, *Δsrv2*, *srv2-189*, and *Δdnm1* cells were determined in YPD/YPR. Increases of OCR (from YPD to YPR) in wild-type, *Δsrv2*, *srv2-189*, and *Δdnm1* cells were 2.34-, 1.53-, 1.47-, and 1.79-fold, respectively. ***p < 0.001 vs. WT cells. (C) Mitochondrial membrane potential of wild-type, Δsrv2, srv2-189, and Δdnm1 yeast in YPD/YPR medium was evaluated by $DiOC_6$ staining followed by flow cytometry. Wild-type (WT) and Δdnm1 yeast cells showed higher mitochondria membrane potentials in YPR medium, but Δsrv2 and srv2-189 yeast cells did not. Increases of $DiOC_6$ intensity (YPD vs. YPR) in WT, Δsrv2, srv2-189, and Δdnm1 were 3.94-, 0.90-, 0.93-, and 3.34-fold, respectively. **p < 0.01 vs. WT cells. Mean values ± SE were obtained by averaging the values of three independent experiments.

mitochondrial dynamics through its function in actin assembly. Deletion of *SRV2* not only changed the network morphology of mitochondria but also affected mitochondrial activity; *Δsrv2* cells with hyperfused mitochondria have a lower spare respiration capacity when compared with wild-type cells. Furthermore, *Δsrv2* cells are unable to increase oxygen consumption and mitochondrial membrane potential as much as wild-type cells when cultured in non-dextrose medium. Based on these findings, we propose that Srv2 serves as a dual-function modulator of both mitochondrial dynamics and activity.

Srv2 was previously known to regulate actin recycling and severing. Both polarized actin cable assembly and patch formation are the major regulatory functions of Srv2/CAP (Toshima et al., 2016). Our results of *SRV2* deletion and mutant alleles bring the regulatory mechanisms of mitochondria and actin dynamics together. The yeast two-hybrid, co-precipitation and BiFC results demonstrated the interaction between Dnm1 and Srv2. The interaction was even preserved under the condition when actin cable assembly was inhibited by latrunculin A. However, deletion of *SRV2* did not affect Dnm1 localized to mitochondria. This result ruled out the possibility that Srv2 involves in mitochondria dynamics by affecting Dnm1 recruitment to mitochondria.

Over-expressed C-terminal Srv2 and the Pfy1-compensated *SRV2* deletion phenotypes demonstrated the involvement of actin in the formation of hyperfused mitochondria in *Δsrv2* cells. Mutant alleles that caused

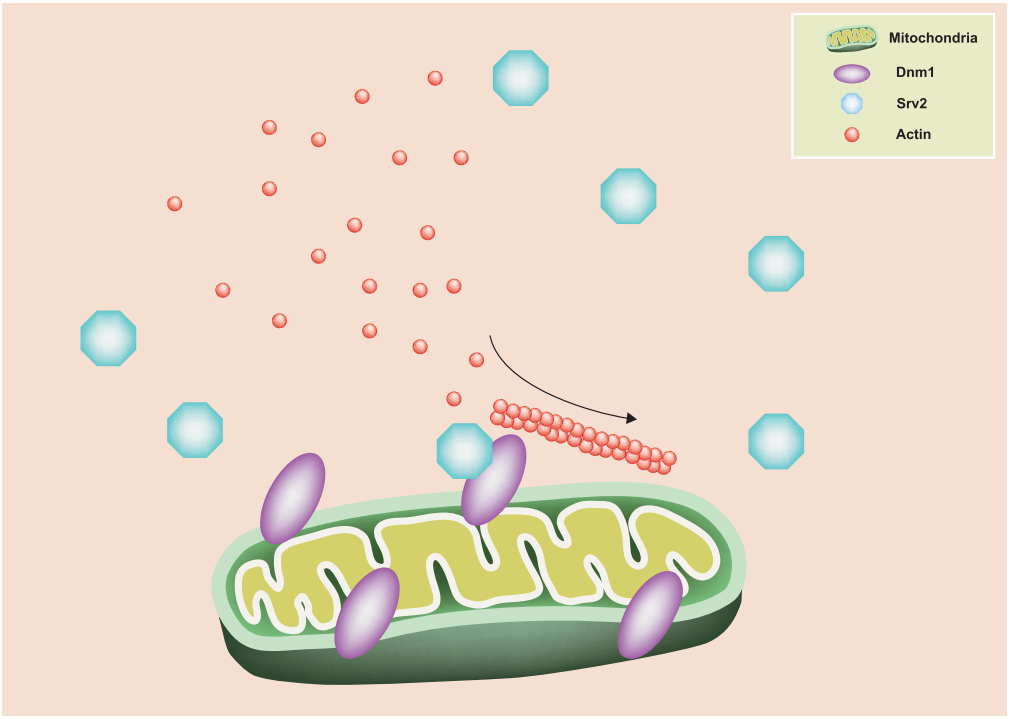

Figure 7. Model of Srv2 Regulating Dynamics and Activity by Modulating Actin Assembly on Mitochondria
The model schematically depicts that the Srv2/Dnm1 interaction facilitates Srv2-mediated modulation of actin polymerization on mitochondria. Actin polymerization is required to regulate mitochondria morphology and activity.

minor reduction of actin cable numbers (*srv2-91* and *srv2-98*) led to lower ratio of cells with hyperfused mitochondria than the one caused severe reduction of actin cable numbers (*srv2-189*). These disrupted actin cable counts in mutant cells along with latrunculin A treatment and *TPM1* deletion resulted in hyperfused mitochondria in wild-type cells, suggesting that actin cable formation plays a critical role in mitochondrial dynamics in yeast cells. This notion was further supported by the fact that the hyperfused-elongated mitochondrial network morphology was not seen in Δ*abp1* or Δ*sla1* strains that bear actin patch formation defects. However, mitochondrial network morphology in double-deletion strains is elongated-hyperfused in *Δsrv2 Δdnm1* cells and fragmented in *Δsrv2 Δfzo1* cells. These phenotypes of double-mutant strains suggested that actin cable plays different roles in mitochondrial fusion and fission processes and that Srv2 may be responsible for the differences. The Dnm1/Srv2 interaction may facilitate actin cable assembly on mitochondria. Loss of Srv2 may not only affect actin assembly but also lead to loss of the interaction between mitochondria and actin. Mitochondrial dynamics and activity would be affected either by their interaction with actin cable or when actin assembly at mitochondria is disrupted. We favor a model in which Srv2 mediates mitochondrial dynamics through its function in promoting actin polymerization and stabilizing actin filaments in conjunction with its ability to interact with the fission protein Dnm1 (Figure 7). Potentially, disrupted actin/mitochondria interaction under *SRV2* deletion causes either mitochondrial transporting defect or incomplete mitochondrial division. We still have not collected enough results to distinguish between the two possibilities.

Both *SRV2* and *DNM1* deletion yeasts possess hyperfused mitochondria with less reserve respiration capacity compared with wild-type cells. The reserve respiration capacity results are in agreement with the mitochondrial membrane potentials measured under conditions without catabolite repression (Figure 6). These data strongly suggest that well-maintained mitochondrial dynamics are required for the proper function of oxidative phosphorylation complexes.

Unexpectedly, the reserve respiration capacities were different in the *Δsrv2* and *Δdnm1* strains, although both strains contained an elongated-hyperfused mitochondrial network. Even so, we found that the morphology of the mitochondrial network was different between *Δsrv2* cells and *Δdnm1* cells. The

mitochondria in *Δsrv2* cells formed an elongated and branched network, whereas in *Δdnm1* cells the mesh form of hyperfused mitochondria dominated. The different network morphologies indicate that unidentified factors are involved in the dynamic balance in these strains. A previous study suggested that the machinery of mitochondrial dynamics is correlated with the wild-type and mutant mtDNA expansion rates (Karavaeva et al., 2017; Osman et al., 2015). We speculate that this may underlie the differential reserve respiration capacities of *Δsrv2* cells and *Δdnm1* cells. However, impacts of different shapes of the network on activity require further study.

Based on phylogenetic analyses, two orthologous CAP proteins in mammalian cells, CAP1 and CAP2, serve similar functions as Srv2 in yeast cells. Although microtubules have been emphasized in mitochondrial dynamics, the role of actin filaments in mitochondrial dynamics in mammalian cells requires further study.

In summary, we have characterized Srv2 as a pro-fission factor that modulates mitochondrial activity. Our work brings the regulatory pathways of actin and mitochondrial dynamics together. As the roles of mitochondrial dynamics in the pathogenesis of neurodegenerative diseases and other diseases are emerging, returning the disrupted equivalence of mitochondrial dynamics to normal will be a potential therapeutic target in the future.

Limitations of the Study

Cytoskeletal systems definitely play a role in mitochondrial dynamics, and mammalian cells have much more sophisticated cytoskeleton systems than yeasts. In addition, mitochondrial transport largely relies on microtubules in mammalian cells. Although we have demonstrated that CAP2-knockout mammalian cells also possess elongated-hyperfused mitochondria, further study is required to clarify how actin assembly on mitochondria is involved in fission and transportation in mammalian cells.

METHODS

All methods can be found in the accompanying Transparent Methods supplemental file.

SUPPLEMENTAL INFORMATION

Supplemental Information includes Transparent Methods, six figures, and two tables and can be found with this article online at https://doi.org/10.1016/j.isci.2018.12.021.

ACKNOWLEDGMENTS

We would like to thank Jin-Jer Lin for his valuable comments on the manuscript, Ann-Shyn Chiang for a microscope objective lens, and David Chan and Janet Shaw for yeast strains. Assistance provided by Jiayee Wu was greatly appreciated. This work was supported by the Ministry of Science and Technology of Taiwan (105-2320-B-007 -005 and 105-2923-B-007 -001 –MY3), Academia Sinica (AS-TP-L107-1), and the Intramural Research Program of the NINDS, NIH.

AUTHOR CONTRIBUTIONS

Conceptualization, Y-.C.C., C.B., and C-.R.C.; Methodology, T-.H.C., C.B., and C-.R.C.; Investigation, Y-.C.C., W-.L.L., C-.L.C., and C-.R.C.; Writing – Original Draft, Y-.C.C. and C-.R.C.; Writing – Review & Editing, C-.R.C. and C.B.; Funding Acquisition, W-.Y.Y., C.B., and C-.R.C.; Resources, T-.H.C., W-.Y.Y., C.B., and C-.R.C.; Supervision, C.B. and C-.R.C.

DECLARATION OF INTERESTS

The authors declare no competing interests.

Received: May 18, 2018
Revised: September 16, 2018
Accepted: December 20, 2018
Published: January 25, 2019

REFERENCES

Alioto, S.L., Garabedian, M.V., Bellavance, D.R., and Goode, B.L. (2016). Tropomyosin and profilin cooperate to promote formin-mediated actin nucleation and drive yeast actin cable assembly. Curr. Biol. *26*, 3230–3237.

Altmann, K., and Westermann, B. (2005). Role of essential genes in mitochondrial morphogenesis in *Saccharomyces cerevisiae*. Mol. Biol. Cell *16*, 5410–5417.

Balcer, H.I., Goodman, A.L., Rodal, A.A., Smith, E., Kugler, J., Heuser, J.E., and Goode, B.L. (2003). Coordinated regulation of actin filament turnover by a high-molecular-weight Srv2/CAP complex, cofilin, profilin, and Aip1. Curr. Biol. *13*, 2159–2169.

Blackstone, C., and Chang, C.-R. (2011). Mitochondria unite to survive. Nat. Cell Biol. *13*, 521–522.

Böckler, S., Chelius, X., Hock, N., Klecker, T., Wolter, M., Weiss, M., Braun, R.J., and Westermann, B. (2017). Fusion, fission, and transport control asymmetric inheritance of mitochondria and protein aggregates. J. Cell Biol. *216*, 2481–2498.

Burman, J.L., Pickles, S., Wang, C., Sekine, S., Vargas, J.N.S., Zhang, Z., Youle, A.M., Nezich, C.L., Wu, X., Hammer, J.A., and Youle, R.J. (2017). Mitochondrial fission facilitates the selective mitophagy of protein aggregates. J. Cell Biol. *216*, 3231–3247.

Castresana, J. (2000). Selection of conserved blocks from multiple alignments for their use in phylogenetic analysis. Mol. Biol. Evol. *17*, 540–552.

Chang, C.-R., and Blackstone, C. (2007). Cyclic AMP-dependent protein kinase phosphorylation of Drp1 regulates its GTPase activity and mitochondrial morphology. J. Biol. Chem. *282*, 21583–21587.

Chaudhry, F., Breitsprecher, D., Little, K., Sharov, G., Sokolova, O., and Goode, B.L. (2013). Srv2/cyclase-associated protein forms hexameric *shurikens* that directly catalyze actin filament severing by cofilin. Mol. Biol. Cell *24*, 31–41.

Chaudhry, F., Jansen, S., Little, K., Suarez, C., Boujemaa-Paterski, R., Blanchoin, L., and Goode, B.L. (2014). Autonomous and *in trans* functions for the two halves of Srv2/CAP in promoting actin turnover. Cytoskeleton (Hoboken) *71*, 351–360.

Chaudhry, F., Little, K., Talarico, L., Quintero-Monzon, O., and Goode, B.L. (2010). A central role for the WH2 domain of Srv2/CAP in recharging actin monomers to drive actin turnover in vitro and in vivo. Cytoskeleton (Hoboken) *67*, 120–133.

Chevenet, F., Brun, C., Banuls, A.-L., Jacq, B., and Christen, R. (2006). TreeDyn: towards dynamic graphics and annotations for analyses of trees. BMC Bioinformatics *7*, 439.

Cho, D.-H., Nakamura, T., Fang, J., Cieplak, P., Godzik, A., Gu, Z., and Lipton, S.A. (2009). S-nitrosylation of Drp1 mediates β-amyloid-related mitochondrial fission and neuronal injury. Science *324*, 102–105.

Dereeper, A., Audic, S., Claverie, J.-M., and Blanc, G. (2010). BLAST-EXPLORER helps you building datasets for phylogenetic analysis. BMC Evol. Biol. *10*, 8.

Dunn, K.W., Kamocka, M.M., and McDonald, J.H. (2011). A practical guide to evaluating colocalization in biological microscopy. Am. J. Physiol. Cell Physiol. *300*, C723–C742.

Edgar, R.C. (2004). MUSCLE: multiple sequence alignment with high accuracy and high throughput. Nucleic Acids Res. *32*, 1792–1797.

Fedor-Chaiken, M., Deschenes, R.J., and Broach, J.R. (1990). *SRV2*, a gene required for *RAS* activation of adenylate cyclase in yeast. Cell *61*, 329–340.

Fehrenbacher, K.L., Yang, H.-C., Gay, A.C., Huckaba, T.M., and Pon, L.A. (2004). Live cell imaging of mitochondrial movement along actin cables in budding yeast. Curr. Biol. *14*, 1996–2004.

Freeman, N.L., Chen, Z., Horenstein, J., Weber, A., and Field, J. (1995). An actin monomer binding activity localizes to the carboxyl-terminal half of the *Saccharomyces cerevisiae* cyclase-associated protein. J. Biol. Chem. *270*, 5680–5685.

Friedman, J.R., Lackner, L.L., West, M., DiBenedetto, J.R., Nunnari, J., and Voeltz, G.K. (2011). ER tubules mark sites of mitochondrial division. Science *334*, 358–362.

Gancedo, J.M. (1998). Yeast carbon catabolite repression. Microbiol. Mol. Biol. Rev. *62*, 334–361.

Gerst, J.E., Ferguson, K., Vojtek, A., Wigler, M., and Field, J. (1991). CAP is a bifunctional component of the *Saccharomyces cerevisiae* adenylyl cyclase complex. Mol. Cell. Biol. *11*, 1248–1257.

Ghaemmaghami, S., Huh, W.-K., Bower, K., Howson, R.W., Belle, A., Dephoure, N., O'Shea, E.K., and Weissman, J.S. (2003). Global analysis of protein expression in yeast. Nature *425*, 737–741.

Gomes, L.C., Di Benedetto, G., and Scorrano, L. (2011). During autophagy mitochondria elongate, are spared from degradation and sustain cell viability. Nat. Cell Biol. *13*, 589–598.

Griffin, E.E., Graumann, J., and Chan, D.C. (2005). The WD40 protein Caf4p is a component of the mitochondrial fission machinery and recruits Dnm1p to mitochondria. J. Cell Biol. *170*, 237–248.

Guindon, S., and Gascuel, O. (2003). A simple, fast, and accurate algorithm to estimate large phylogenies by maximum likelihood. Syst. Biol. *52*, 696–704.

Gurel, P.S., Mu, A., Guo, B., Shu, R., Mierke, D.F., and Higgs, H.N. (2015). Assembly and turnover of short actin filaments by the formin INF2 and profilin. J. Biol. Chem. *290*, 22494–22506.

Haarer, B.K., Lillie, S.H., Adams, A.E.M., Magdolen, V., Bandlow, W., and Brown, S.S. (1990). Purification of profilin from *Saccharomyces cerevisiae* and analysis of profilin-deficient cells. J. Cell Biol. *110*, 105–114.

Hatch, A.L., Gurel, P.S., and Higgs, H.N. (2014). Novel roles for actin in mitochondrial fission. J. Cell Sci. *127*, 4549–4560.

Hatch, A.L., Ji, W.-K., Merrill, R.A., Strack, S., and Higgs, H.N. (2016). Actin filaments as dynamic reservoirs for Drp1 recruitment. Mol. Biol. Cell *27*, 3109–3121.

Hermann, G.J., Thatcher, J.W., Mills, J.P., Hales, K.G., Fuller, M.T., Nunnari, J., and Shaw, J.M. (1998). Mitochondrial fusion in yeast requires the transmembrane GTPase Fzo1p. J. Cell Biol. *143*, 359–373.

Higuchi-Sanabria, R., Vevea, J.D., Charalel, J.K., Sapar, M.L., and Pon, L.A. (2016). The transcriptional repressor Sum1p counteracts Sir2p in regulation of the actin cytoskeleton, mitochondrial quality control and replicative lifespan in *Saccharomyces cerevisiae*. Microb. Cell *3*, 79–88.

Huckaba, T.M., Gay, A.C., Pantalena, L.F., Yang, H.-C., and Pon, L.A. (2004). Live cell imaging of the assembly, disassembly, and actin cable-dependent movement of endosomes and actin patches in the budding yeast, *Saccharomyces cerevisiae*. J. Cell Biol. *167*, 519–530.

Ji, W.-k., Hatch, A.L., Merrill, R.A., Strack, S., and Higgs, H.N. (2015). Actin filaments target the oligomeric maturation of the dynamin GTPase Drp1 to mitochondrial fission sites. Elife *4*, e11553.

Jin, S.M., and Youle, R.J. (2012). PINK1- and Parkin-mediated mitophagy at a glance. J. Cell Sci. *125*, 795–799.

Karavaeva, I.E., Golyshev, S.A., Smirnova, E.A., Sokolov, S.S., Severin, F.F., and Knorre, D.A. (2017). Mitochondrial depolarization in yeast zygotes inhibits clonal expansion of selfish mtDNA. J. Cell Sci. *130*, 1274–1284.

Koch, A., Schneider, G., Lüers, G.H., and Schrader, M. (2004). Peroxisome elongation and constriction but not fission can occur independently of dynamin-like protein 1. J. Cell Sci. *117*, 3995–4006.

Kuravi, K., Nagotu, S., Krikken, A.M., Sjollema, K., Deckers, M., Erdmann, R., Veenhuis, M., and van der Klei, I.J. (2006). Dynamin-related proteins Vps1p and Dnm1p control peroxisome abundance in *Saccharomyces cerevisiae*. J. Cell Sci. *119*, 3994–4001.

Lee, J.E., Westrate, L.M., Wu, H., Page, C., and Voeltz, G.K. (2016). Multiple dynamin family members collaborate to drive mitochondrial division. Nature *540*, 139–143.

Legesse-Miller, A., Massol, R.H., and Kirchhausen, T. (2003). Constriction and Dnm1p recruitment are distinct processes in mitochondrial fission. Mol. Biol. Cell *14*, 1953–1963.

Li, S., Xu, S., Roelofs, B.A., Boyman, L., Lederer, W.J., Sesaki, H., and Karbowski, M. (2015). Transient assembly of F-actin on the outer mitochondrial membrane contributes to mitochondrial fission. J. Cell Biol. *208*, 109–123.

Liu, H., and Bretscher, A. (1989). Disruption of the single tropomyosin gene in yeast results in the disappearance of actin cables from the cytoskeleton. Cell *57*, 233–242.

Magdolen, V., Drubin, D.G., Mages, G., and Bandlow, W. (1993). High levels of profilin suppress the lethality caused by overproduction of actin in yeast cells. FEBS Lett. *316*, 41–47.

Mattila, P.K., Quintero-Monzon, O., Kugler, J., Moseley, J.B., Almo, S.C., Lappalainen, P., and Goode, B.L. (2004). A high-affinity interaction with ADP-actin monomers underlies the mechanism and in vivo function of Srv2/cyclase-associated protein. Mol. Biol. Cell *15*, 5158–5171.

Moore, A.S., Wong, Y.C., Simpson, C.L., and Holzbaur, E.L.F. (2016). Dynamic actin cycling through mitochondrial subpopulations locally regulates the fission-fusion balance within mitochondrial networks. Nat. Commun. *7*, 12886.

Mozdy, A.D., McCaffery, J.M., and Shaw, J.M. (2000). Dnm1p GTPase-mediated mitochondrial fission is a multi-step process requiring the novel integral membrane component Fis1p. J. Cell Biol. *151*, 367–380.

Narendra, D., Tanaka, A., Suen, D.-F., and Youle, R.J. (2009). Parkin-induced mitophagy in the pathogenesis of Parkinson disease. Autophagy *5*, 706–708.

Narendra, D.P., Jin, S.M., Tanaka, A., Suen, D.-F., Gautier, C.A., Shen, J., Cookson, M.R., and Youle, R.J. (2010). PINK1 is selectively stabilized on impaired mitochondria to activate Parkin. PLoS Biol. *8*, e1000298.

Osman, C., Noriega, T.R., Okreglak, V., Fung, J.C., and Walter, P. (2015). Integrity of the yeast mitochondrial genome, but not its distribution and inheritance, relies on mitochondrial fission and fusion. Proc. Natl. Acad. Sci. U S A *112*, E947–E956.

Peche, V., Shekar, S., Leichter, M., Korte, H., Schröder, R., Schleicher, M., Holak, T.A., Clemen, C.S., Ramanath-Y, B., Pfitzer, G., et al. (2007). CAP2, cyclase-associated protein 2, is a dual compartment protein. Cell. Mol. Life Sci. *64*, 2702–2715.

Sagot, I., Rodal, A.A., Moseley, J., Goode, B.L., and Pellman, D. (2002). An actin nucleation mechanism mediated by Bni1 and profilin. Nat. Cell Biol. *4*, 626–631.

Sesaki, H., and Jensen, R.E. (2001). *UGO1* encodes an outer membrane protein required for mitochondrial fusion. J. Cell Biol. *152*, 1123–1134.

Shirendeb, U.P., Calkins, M.J., Manczak, M., Anekonda, V., Dufour, B., McBride, J.L., Mao, P., and Reddy, P.H. (2012). Mutant huntingtin's interaction with mitochondrial protein Drp1 impairs mitochondrial biogenesis and causes defective axonal transport and synaptic degeneration in Huntington's disease. Hum. Mol. Genet. *21*, 406–420.

Skarp, K.-P., Zhao, X., Weber, M., and Jäntti, J. (2008). Use of bimolecular fluorescence complementation in yeast *Saccharomyces cerevisiae*. Methods Mol. Biol. *457*, 165–175.

Toshima, J.Y., Horikomi, C., Okada, A., Hatori, M.N., Nagano, M., Masuda, A., Yamamoto, W., Siekhaus, D.E., and Toshima, J. (2016). Srv2/CAP is required for polarized actin cable assembly and patch internalization during clathrin-mediated endocytosis. J. Cell Sci. *129*, 367–379.

Vojtek, A., Haarer, B., Field, J., Gerst, J., Pollard, T.D., Brown, S., and Wigler, M. (1991). Evidence for a functional link between profilin and CAP in the yeast S. cerevisiae. Cell *66*, 497–505.

Westermann, B. (2010). Mitochondrial dynamics in model organisms: what yeasts, worms and flies have taught us about fusion and fission of mitochondria. Semin. Cell Dev. Biol. *21*, 542–549.

Westermann, B., and Neupert, W. (2000). Mitochondria-targeted green fluorescent proteins: convenient tools for the study of organelle biogenesis in *Saccharomyces cerevisiae*. Yeast *16*, 1421–1427.

Wong, E.D., Wagner, J.A., Gorsich, S.W., McCaffery, J.M., Shaw, J.M., and Nunnari, J. (2000). The dynamin-related GTPase, Mgm1p, is an intermembrane space protein required for maintenance of fusion competent mitochondria. J. Cell Biol. *151*, 341–352.

Yoshida, M., Ohnuki, S., Yashiroda, Y., and Ohya, Y. (2013). Profilin is required for Ca^{2+} homeostasis and Ca^{2+}-modulated bud formation in yeast. Mol. Genet. Genomics *288*, 317–328.

Youle, R.J., and van der Bliek, A.M. (2012). Mitochondrial fission, fusion, and stress. Science *337*, 1062–1065.

Zhu, P.-P., Patterson, A., Stadler, J., Seeburg, D.P., Sheng, M., and Blackstone, C. (2004). Intra- and intermolecular domain interactions of the C-terminal GTPase effector domain of the multimeric dynamin-like GTPase Drp1. J. Biol. Chem. *279*, 35967–35974.

ISCI, Volume *11*

Supplemental Information

Srv2 Is a Pro-fission Factor that Modulates Yeast Mitochondrial Morphology and Respiration by Regulating Actin Assembly

Ying-Chieh Chen, Tzu-Hao Cheng, Wei-Ling Lin, Chang-Lin Chen, Wei Yuan Yang, Craig Blackstone, and Chuang-Rung Chang

Supplemental Figure 1.

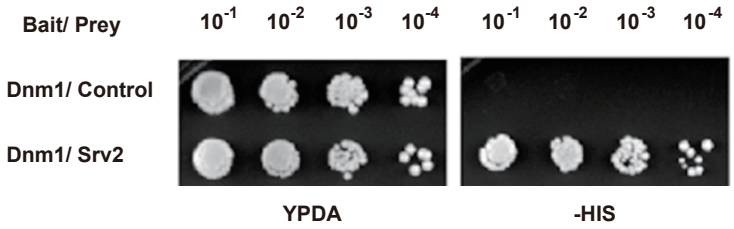

Figure S1. Yeast two-hybrid analysis to identify Srv2-Dnm1 interaction, related to Figure 1.

Yeast two-hybrid system LexABD/ Gal4AD was used to assess protein interaction. The interaction between proteins fused with LexABD and Gal4AD drives reporter gene "HIS3" expression. Yeast cells expressing fusion protein LexABD-Dnm1 and Gal4AD-Srv2 were assayed for growth on SD-His plate (serial dilution as indicated at the top).

.

Supplemental Figure 2.

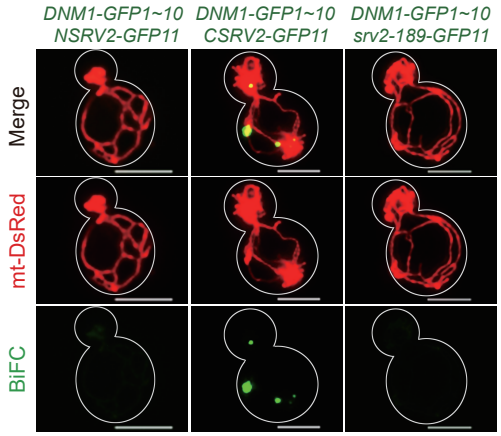

Figure S2. BiFC analysis for assessing interaction between truncated/ mutated Srv2 and Dnm1, related to Figure 1.

Bimolecular fluorescence complementation (BiFC) experiments were used to analyze interaction between N/C-terminal Srv2 and *srv2-189* and Dnm1. Yeast transformed with DNM1-GFP1~10+ NSRV2-GFP11, DNM1-GFP1~10+ CSRV2-GFP11, or DNM1-GFP1~10+ *srv2-189*-GFP11 were examined using BiFC assays. To improve the poor BiFC signals, NSRV2-GFP11/ CSRV2-GFP11/ *srv2-189*-GFP11 were expressed by pRS425 vector (2-micron plasmid). mt-DsRed was expressed to label mitochondria. Scale bars denote 5 μm.

Supplemental Figure 3.

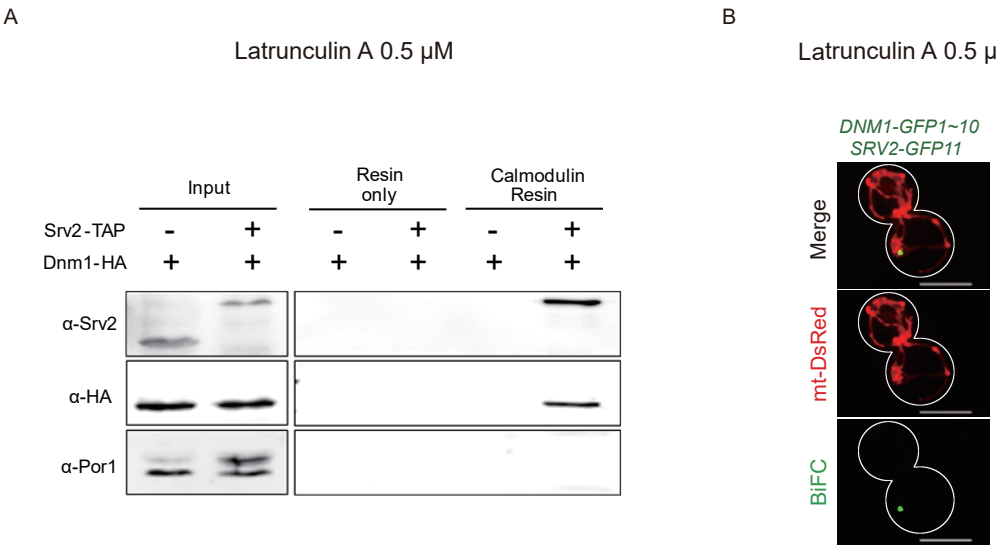

Figure S3. Latrunculin A treatment does not disrupt Srv2-Dnm1 interaction, related to Figure 5.

Co-Immunoprecipitation (Co-IP) and bimolecular fluorescence complementation (BiFC) combined with latrunculin A (Lat-A) were used to assess Srv2 Dnm1 interaction upon disrupted actin dynamics. (A) The same strains and materials as in Figure 1B combined with 0.5 μM Lat-A were used to perform Co-IP experiments. (B) Yeast transformed with SRV2-GFP11 and DNM1-GFP1~10 combined 0.5 μM Lat-A were used to perform BiFC experiments. The results indicated that 0.5 μM Lat-A does not disrupt Srv2-Dnm1 interaction.

Supplemental Figure 4.

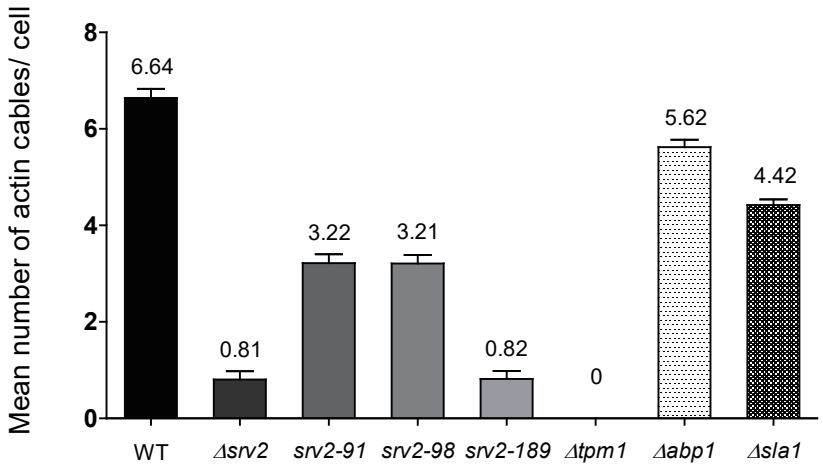

Figure S4. Actin cable counts in different yeast strains, related to Figure 5.

WT, *srv2* mutants, actin cable mutant (*Δtpm1*) and actin patch mutants (*Δabp1* and *Δsla1*) were grown at 30 °C in YPD, fixed and stained with rhodamine phalloidin. Visible actin cables in mother cell were counted (n≧50 cells per strain).

Supplemental Figure 5.

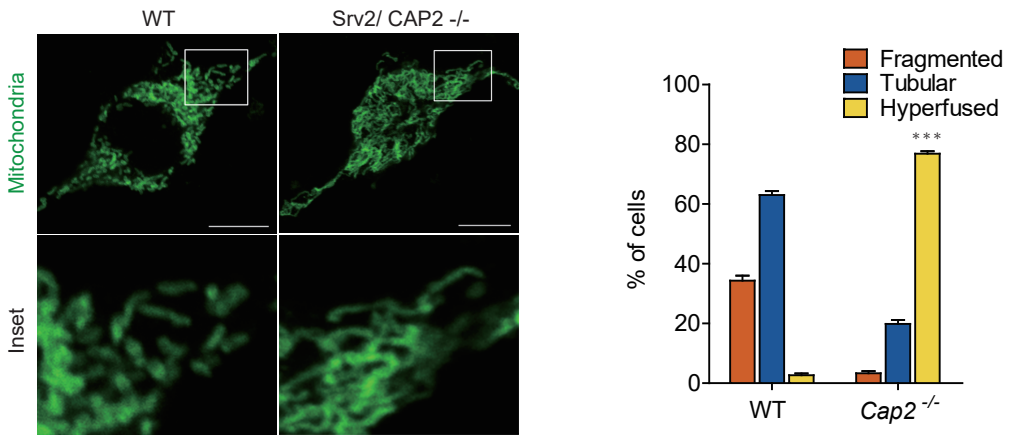

Figure S5. Mitochondrial elongation and hyperfusion in CAP2-/- Human neuroblastoma SH-SY5Y cell line, related to Figure 2.

The CAP2$^{-/-}$ SH-SY5Y cell line was generated by CRISPR/ Cas9 system. Mitochondrial network morphology in wild-type (WT) and CAP2$^{-/-}$ cells expressing mito-EYFP was examined by fluorescence microscopy. The ratios of WT and CAP2$^{-/-}$ cells with hyperfused mitochondria were: WT, 2.67 % and CAP2$^{-/-}$, 76.83 %. Statistical data for each strain were obtained from three trials of 100 cells. The mean values ± SE were obtained by averaging the percentages of three counts. ***$p<0.001$ vs. WT group. Scale bars denote 10 μm.

Supplemental Figure 6.

A

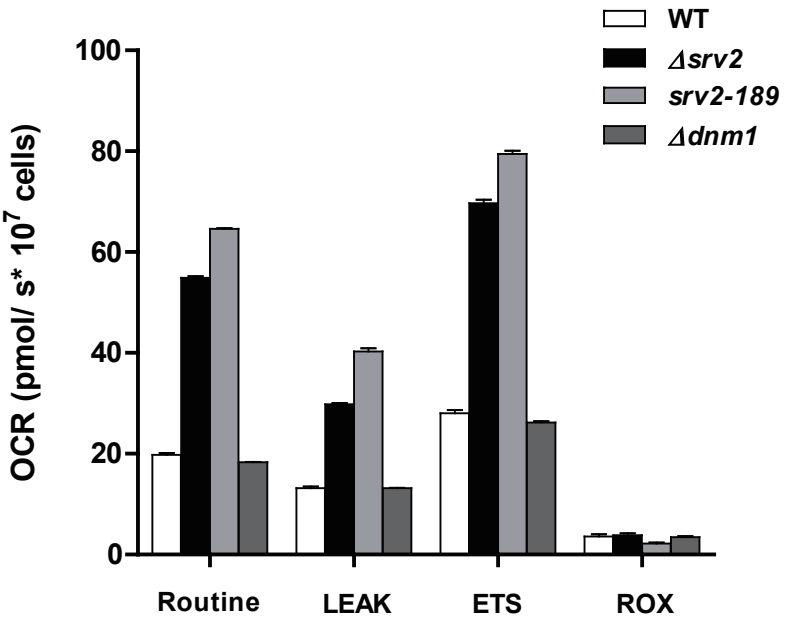

Figure S6 Oxygen consumption rates (OCR) are different among yeast strains, related to Figure 6.

OCR in different yeast strains under basal conditions or the addition of TET (ATP synthetase inhibitor), FCCP (uncoupler, proton carrier), and Antimycin A (complex III inhibitor) were measured by high resolution respirometry. Routine denotes OCR in the basal condition. LEAK denotes OCR with TET treatment, which reflects futile oxygen consumption even though ATP synthesis is blocked. ETS denotes OCR after FCCP titration, which causes proton loss and drive mitochondria consume more oxygen to replenish the proton gradient. ROX denotes OCR in Antimycin A treatment, which depletes OCR derived from mitochondria respiration and reveals oxygen consumption in this system other than mitochondria.

Supplemental Table 1. Yeast strains and their genotypes used in this study, related to Figure 1, 2, 3, 4, 5 and 6.

Strain	Genotype
WT	W303-1A
Δ*srv2*	W303-1A, Δ*srv2:: KanMX*
HIS3::SRV2	W303-1A Δ*srv2:: KanMX pSRV2::HIS3*
Gal::SRV2	W303-1A, Δ*srv2:: KanMX GalSpSRV2::HIS3*
Δ*dnm1*	W303-1A, Δ*dnm1::HPH*
Δ*fzo1*	W303-1A, Δ*fzo1:: HPH*
Δ*srv2*Δ*dnm1*	W303-1A, Δ*srv2:: KanMX* Δ*dnm1::HPH*
Δ*srv2*Δ*fzo1*	W303-1A, Δ*srv2:: KanMX* Δ*fzo1::HPH*
srv2-91	W303-1A, Δ*srv2:: KanMX psrv2-91::HIS3*
srv2-98	W303-1A, Δ*srv2:: KanMX psrv2-98::HIS3*
srv2-189	W303-1A, Δ*srv2:: KanMX psrv2-189::HIS3*
DNM1-HA	JSY1542
SRV2-TAP, DNM1-HA	JSY1542, *SRV2-TAP::HIS3MX6*
Δ*srv2, DNM1-HA*	JSY1542, Δ*srv2:: KanMX*
DNM1-GFP	W303-1A, *DNM1-GFP::HIS3MX*
Δ*srv2, DNM1-GFP*	W303-1A, Δ*srv2:: KAN DNM1-GFP::HIS3MX*
Δ*fis1, DNM1-GFP*	W303-1A, Δ*fis1:: HPH DNM1-GFP::HIS3MX*
Δ*tpm1*	W303-1A, Δ*tpm1::KanMX*
Δ*abp1*	W303-1A, Δ*abp1::KanMX*
Δ*sla1*	W303-1A, Δ*sla1::KanMX*

Supplemental Table 2. Plasmids used in this study, related to Figure 1, 2, 3, 4 and 5.

Plasmid ID	Description
pVT100U-mtGFP	Matrix-targeted GFP expression
pVT100U-mtDsRed	Matrix-targeted DsRed expression
pRS403-pSRV2	For *SRV2* gene integration
pRS403-GalSSRV2	For *GalSpSRV2* integration
pRS403-psrv2-91	For *srv2-91* allele integration
pRS403-psrv2-98	For *srv2-98* allele integration
pRS403-psrv2-189	For *srv2-189* allele integration
pRS425-ADH-NSRV2	For N-terminal Srv2 overexpression
pRS425-ADH-CSRV2	For C-terminal Srv2 overexpression
pRS425-ADH-PFY1	For Pfy1 overexpression
pRS413-pSRV2-GFP11	For Bimolecular fluorescence complementation
pRS414-pDNM1-GFP1-10	For Bimolecular fluorescence complementation
pRS414-pFZO1-GFP1-10	For Bimolecular fluorescence complementation
pRS425-pNSRV2-GFP11	For Bimolecular fluorescence complementation
pRS425-pCSRV2-GFP11	For Bimolecular fluorescence complementation
pRS425-psrv2-189-GFP11	For Bimolecular fluorescence complementation

Transparent Methods

Yeast Strains and Genotypes

All yeast strains and genotypes used in this study are listed in Supplemental Table 1. Gene deletion strains and *DNM1-GFP* tag-related strains were constructed based on *S. cerevisiae* W303-1A (RRID: SCR_003093). Gene deletion strains were constructed mainly by PCR-based gene replacement with a *KanMX4* cassette that was amplified from the yeast deletion collection. For double-gene deletion strains, the *KanMX4* cassette was replaced by *HIS3MX6* or *HphMX4* cassettes from a yeast GFP collection or pAG32. The *KanMX4* cassette was then used again to construct the second gene deletion. For *DNM1-GFP* fusion strains, *GFP* with a *HIS3MX6* cassette was integrated proximal to the stop codon of *DNM1* by PCR-mediated homologous recombination. For construction of strains CYC005, CYC016, CYC018, and CYC046, the integrative plasmids pRS403-*pSRV2*, pRS403-*psrv2-91*, pRS403-*psrv2-98*, and pRS403-*GalSpSRV2* were linearized by restriction digestion for integration at the *HIS3* locus after yeast transformation.

Plasmid Constructions

All plasmids used in this study are listed in Supplemental Table 2. pRS425-ADH1 was constructed by amplifying the *ADH1* promoter from pGAD424 and cloning into

pRS425. Subsequently, DNA fragments encoding *N-SRV2* (residues 1-259), *C-SRV2* (residues 253-526), and *PFY1* were amplified from yeast genomic DNA and then cloned into pRS425-ADH1 to generate pRS425-ADH1-*N-SRV2,* pRS425-ADH1-*C-SRV2*, and pRS425-ADH1-*PFY1*. pRS403-*pSRV2* was constructed by amplifying the open reading frame (ORF) of the *SRV2* gene along with the upstream 490 base pairs from yeast genomic DNA and cloning into the pRS403 vector. Based on previous studies (Chaudhry et al., 2010, Chaudhry et al., 2013), pRS403-*psrv2-91* and pRS403-*psrv2-98* were generated by PCR-mediated mutagenesis from pRS403-*pSRV2* using primers (*srv2-91*: CACAGTTTTGGACTAATGCTATTGCTGCTGCTTACAGAGAGTCTGATC and GATCAGACTCTCTGTAAGCAGCAGCAATAGCATTAGTCCAAAACTGTG/ *srv2-98*: GAAAATATCACTAAGGGTGCTGCTGCTGCTGACAAATCCCAACAAAC and GTTTGTTGGGATTTGTCAGCAGCAGCAGCACCCTTAGTGATATTTTC). pRS403-*psrv2-189* was generated by PCR-mediated mutagenesis with both sets of primers. For construction of pRS403-*GalSpSRV2*, the DNA fragment containing the *GalS* promoter and *SRV2* ORF was amplified from pRS414-*GalSpSRV2*. For pVT100U-mtDsRed construction, the GFP in pVT100U-mtGFP was replaced by a DsRed sequence amplified from DCY2370 (the yeast strain containing *DNM1-GFP*

and mtDsRed, a gift of Dr. David Chan, California Institute of Technology). For plasmids used in the bimolecular fluorescence complementation (BiFC) assay, DNA fragments of split-GFP (GFP1-10/ GFP11) were amplified from pcDNA3.1-MFN2-sfGFP11 and pcDNA3.1-sfGFP1~10 (gifts from Dr. Tzu Kang Sang, National Tsing Hua University). DNA fragments encoding individual proteins and native promoters were ligated to either GFP1-10 or GFP11 DNA fragments. Ligated DNA fragments were cloned into pRS413 and pRS414 (low-copy vectors), as shown in Supplemental Table 2.

Microscopy

Yeasts were examined during the log phase of growth in medium containing either glucose or galactose. Fluorescence images were captured using an inverted microscope (Zeiss/Observer.Z1) with a 63× objective lens (Zeiss Plan-ApoChromat 63×) and AxioVs40 software. Mitochondria were visualized by expressing matrix-targeted Su9-EGFP from pVT100-mtGFP (Westermann and Neupert, 2000) or matrix-targeted Su9-DsRed from pVT100-mtDsRed. For colocalization analysis of Dnm1 and mitochondria, *z*-section images captured by fluorescence microscopy were projected (orthogonal projection, maximum) using ZEN 2012 image acquisition software. Each individual yeast cell in the projected image was analyzed separately

with ImageJ software (NIH) and the plugin “Manders Coefficients”. For actin cable and patch staining, yeasts were fixed in medium containing 3.7% formaldehyde for 15 min at room temperature, washed with phosphate buffered saline (PBS), and stained in PBS containing 0.165 μM rhodamine phalloidin. Actin cable counts were based on the previous published paper (Alioto et al., 2016, Higuchi-Sanabria et al., 2016). For latrunculin A treatment, yeast cells were incubated with medium containing 0.5 μM latrunculin A for 6 h. For galactose induction, CYC005 was inoculated in SC medium containing 2% raffinose until the log phase of growth. The yeast cells were then transferred to YP medium containing 2% galactose for 3 h.

Tandem affinity purification (TAP) tag co-precipitation

Yeasts with TAP tag grown to mid-log phase were harvested by centrifugation. Pellets were washed with ddH_2O and resuspended with extraction buffer (10 mM Tris-Cl, pH 8.0, 1 mM dithiothreitol (DTT), 150 mM NaCl, 1 mM magnesium acetate, 1 mM imidazole, 2 mM $CaCl_2$, 0.1% NP-40). Glass beads were added to break the yeast cells during vortexing for 15 min at 4 °C. Supernatants were collected thoroughly from cell lysates by centrifugation at 15,000 *g*. Aliquots (150 μL) of the resulting supernatant were incubated with 25 μL of bovine serum albumin pre-coated calmodulin Sepharose beads for 3 hr at 4 °C. After incubation, the Sepharose beads were washed

three times with wash buffer (10 mM Tris-Cl, pH 8.0, 1 mM DTT, 500 mM NaCl, 1 mM magnesium acetate, 1 mM imidazole, 2 mM $CaCl_2$, 0.1% NP-40). The Sepharose beads were incubated with elution buffer (10 mM Tris-Cl, pH 8.0, 1 mM DTT, 150 mM NaCl, 1 mM magnesium acetate, 1 mM imidazole, 2 mM EGTA, 0.1% NP-40) for 5 min. The Sepharose beads with elution buffer and protein sample buffer were boiled for 5 min and cooled. The supernatants were collected for further western blot analysis.

BiFC Assay

To detect specific interaction between Srv2 and Dnm1 in yeasts, plasmids pRS413-pSRV2-GFP11 and pRS414-pDNM1-GFP1-10 were transformed in the specific strains described; the plasmids were constructed with low-copy vectors (yeast centromere plasmids) and native promoter. To avoid the titration effects of endogenous protein (without the split-GFP moiety), the indicated gene deletion strains were used in these experiments. For example, the Δsrv2 Δdnm1 yeast strain transformed with pRS413-pSRV2-GFP11 and pRS414-pDNM1-GFP1-10 was used to detect the interaction of Srv2 and Dnm1. pVT100-mtDsRed was also used for labeling mitochondria.

Mitochondrial Fractionation

Mitochondria crude extracts were obtained by yeast cell fractionation (Meisinger et al., 2006). Briefly, yeast cells grown to mid-log phase were harvested by centrifugation at 1,500 g and suspended in DTT buffer at 30 °C for 20 min. The cells were washed and resuspended in buffer containing zymolyase for 30 min. Zymolyase-treated yeasts (spheroplasts) were collected by centrifugation, resuspended in homogenization buffer, and homogenized with 15 strokes of a glass-Teflon homogenizer. The homogenates were centrifuged at 1,500 g to pellet cell debris and nuclei, and the supernatants were collected and centrifuged at 4,000 g and then at 12,000 g. The pellets were denoted as the "crude mitochondria fraction", and supernatants were denoted as the "cytosolic fraction". Protein in both fractions were then analyzed by western blotting.

Flow Cytometry

Mitochondrial membrane potential was evaluated by DiOC6(3) staining (Cat. D273, Life Technology). Yeasts were incubated in medium containing 175 nM DiOC6 (3) for 20 min at 30 °C in the dark. Samples were evaluated using an Accuri C6 flow cytometer (BD Bioscience) following the protocol provided by the company. Data were analyzed using Cellquest software from BD Bioscience.

High-resolution Respirometry

Yeasts oxygen consumption rates were determined using an Oxygraph-2K (Oroboros). Data was analyzed by DatLab software provided by the company. Yeasts grown to stationary phase in Yeast Extract Peptone Dextrose Medium (YPD) were subcultured (160× dilution) in YPD/YPR (raffinose as carbon source) until an optical density at 600 nm of 0.6. The inoculates were then mixed with YPD/ YPR at a concentration of 5 × 10^6 cells per mL. The examination was done using 10^7 cells. Triethyltin bromide (TET, 150 μM), carbonilcyanide p-triflouromethoxyphenylhydrazone (FCCP, < 4 μM), and 2 μM antimycin A were added stepwise. Mitochondrial basal respiration (R), proton leakage (L), and maximal respiration (E) can be evaluated by determining oxygen consumption rates with these mitochondrial inhibitors. To compare the mitochondrial functionality of yeast strains with different basal respiration (routine oxygen consumption), the oxygen consumption rates were transferred to comparable values, designated as the reserve capacity, by calculating (E-R)/E.

Phylogenetic Analysis

Protein sequences of the indicated species were obtained from the Uniprot website (http://www.uniprot.org/). These sequences were aligned, curated, and

phylogenetically analyzed using the MUSCLE online software, Gblocks, and PhyML, respectively (Edgar, 2004, Castresana, 2000, Dereeper et al., 2010, Guindon and Gascuel, 2003). The phylogenetic tree was generated using TreeDyn (Chevenet et al., 2006). Software was accessed at http://www.phylogeny.fr/.

Statistical Analysis

All experiments were conducted with at least three independent trials. To classify mitochondrial morphology, more than 100 cells were examined in each trial. Data are expressed as mean values. All error bars in the figures represented standard error unless otherwise specified. Significance was determined using two-tailed, unpaired Student's *t* tests.

Supplemental References

ALIOTO, S. L., GARABEDIAN, M. V., BELLAVANCE, D. R. & GOODE, B. L. 2016. Tropomyosin and Profilin Cooperate to Promote Formin-Mediated Actin Nucleation and Drive Yeast Actin Cable Assembly. *Curr Biol,* 26**,** 3230-3237.

CASTRESANA, J. 2000. Selection of conserved blocks from multiple alignments for their use in phylogenetic analysis. *Mol Biol Evol,* 17**,** 540-52.

CHAUDHRY, F., BREITSPRECHER, D., LITTLE, K., SHAROV, G., SOKOLOVA, O. & GOODE, B. L. 2013. Srv2/cyclase-associated protein forms hexameric shurikens that directly catalyze actin filament severing by cofilin. *Mol Biol Cell,* 24**,** 31-41.

CHAUDHRY, F., LITTLE, K., TALARICO, L., QUINTERO-MONZON, O. & GOODE, B. L. 2010. A central role for the WH2 domain of Srv2/CAP in recharging actin monomers to drive actin turnover in vitro and in vivo. *Cytoskeleton (Hoboken),* 67**,** 120-33.

CHEVENET, F., BRUN, C., BANULS, A. L., JACQ, B. & CHRISTEN, R. 2006. TreeDyn: towards dynamic graphics and annotations for analyses of trees. *BMC Bioinformatics,* 7**,** 439.

DEREEPER, A., AUDIC, S., CLAVERIE, J. M. & BLANC, G. 2010. BLAST-EXPLORER helps you building datasets for phylogenetic analysis. *BMC Evol Biol,* 10**,** 8.

EDGAR, R. C. 2004. MUSCLE: multiple sequence alignment with high accuracy and high throughput. *Nucleic Acids Res,* 32**,** 1792-7.

GUINDON, S. & GASCUEL, O. 2003. A simple, fast, and accurate algorithm to estimate large phylogenies by maximum likelihood. *Syst Biol,* 52**,** 696-704.

HIGUCHI-SANABRIA, R., VEVEA, J. D., CHARALEL, J. K., SAPAR, M. L. & PON, L. A. 2016. The transcriptional repressor Sum1p counteracts Sir2p in regulation of the actin cytoskeleton, mitochondrial quality control and replicative lifespan in Saccharomyces cerevisiae. *Microb Cell,* 3**,** 79-88.